Correlation between Near-Field Enhancement and Dephasing Time in Plasmonic Dimers

Yaolong Li,[1,2,*] Quan Sun,[2,3,*] Shuai Zu,[2] Xu Shi,[2] Yunquan Liu,[1,4] Xiaoyong Hu,[1,4] Kosei Ueno,[2,§] Qihuang Gong,[1,4,†] and Hiroaki Misawa[2,5,‡]

[1]*State Key Laboratory for Mesoscopic Physics, Frontiers Science Center for Nano-optoelectronics, and Collaborative Innovation Center of Quantum Matter, Department of Physics, Peking University, Beijing 100871, China*

[2]*Research Institute for Electronic Science, Hokkaido University, Sapporo 001-0021, Japan*

[3]*College of Electronic Science & Engineering, Jilin University, Changchun 130012, China*

[4]*Collaborative Innovation Center of Extreme Optics, Shanxi University, Taiyuan, Shanxi 030006, China*

[5]*Center for Emergent Functional Matter Science, National Chiao Tung University, Hsinchu 30010, Taiwan*

(Received 7 October 2019; accepted 26 March 2020; published 24 April 2020)

Near-field enhancement and dephasing time play critical roles in several applications of localized surface plasmon resonance. Here, using an example gold dimer system, we reveal the correlation between the near-field enhancement and dephasing time via time-resolved photoemission electron microscopy. Compared with isolated particles, dimers with small gap sizes show stronger near-field enhancement and shorter dephasing times. These results are well reproduced by numerical simulations and further explained by a coupled dipole approximation model. The roles of near- and far-field coupling and plasmon localization in balancing near-field enhancement and dephasing time are also unveiled.

DOI: 10.1103/PhysRevLett.124.163901

Localized surface plasmon resonance (LSPR) supported by metallic nanoparticles is employed in a wide range of applications that include surface-enhanced Raman scattering (SERS) [1,2], optical trapping [3,4], sensing [5,6], energy harvesting [7,8], and photocatalysis [9,10]. The fascinating optical properties of LSPRs, among which near-field enhancement and dephasing time are two key parameters, play important roles in their various applications. The near-field enhancement of LSPRs is dependent on particle shape, size, arrangement, material, etc. [11–14]. The dephasing time of LSPRs depends on plasmon decay channels, including radiative decay, namely, coupling to photons via scattering, nonradiative decay via interband and intraband excitation, surface electron scattering, and energy or charge transfer [15–17]. In some applications, such as SERS and optical trapping, near-field enhancement is crucial [3,13], while the dephasing time is emphasized in others such as sensing because of its link to the linewidth (Q factor) of the LSPR mode [18]. For energy harvesting and photocatalysis, however, both near-field enhancement and dephasing time are thought to play important roles in increasing the coupling efficiency as well as in the optimization of energy and charge transfer rates [9]. However, the near-field enhancement and dephasing times of plasmonic nanoparticles have not been investigated coordinately, especially in coupled plasmonic systems.

Near-field enhancement of plasmonic dimers, which are the simplest coupled plasmonic systems, has been intensively investigated by numerical simulation [19], indirectly by SERS [13], and directly by photoemission electron microscopy (PEEM) [20,21]. The dephasing times of plasmonic dimers have been investigated via far-field spectral linewidth measurement [15], and directly, in the time domain, via autocorrelation measurements based on third harmonic generation (THG) or multiphoton processes [22–24]. Dephasing times of plasmonic dimers as short as 2 fs have been reported using interferometric THG autocorrelation [22]. However, the dependence of dephasing time on gap size, and more importantly, the correlation between near-field enhancement and dephasing time is unclear.

In this Letter, we describe an experimental investigation into the localized surface plasmon modes of gold (Au) nanoparticle dimers by time-resolved PEEM (TR-PEEM). TR-PEEM has been demonstrated to be a powerful platform for the investigation of the near-field properties and dynamics of LSPRs [25–32]. We report a comprehensive study of the near-field enhancement and dephasing times of plasmonic dimers using wavelength-dependent and time-resolved PEEM measurements. We find that near-field enhancement and dephasing time are dependent on gap size and polarization, owing to the underlying plasmon localization and coupling. Strong near-field enhancement and short dephasing times are observed for small gap sizes with longitudinal polarization. Conversely, weak near-field enhancement is observed for the transverse polarization, but dephasing times are still quite short.

We fabricated an array of isolated disks (diameter $D = 175$ nm, height $H = 30$ nm) and a series of dimer arrays with different gap sizes using electron-beam lithography followed by metal sputtering and a lift-off process (see Supplemental Material [33]). The structure of the

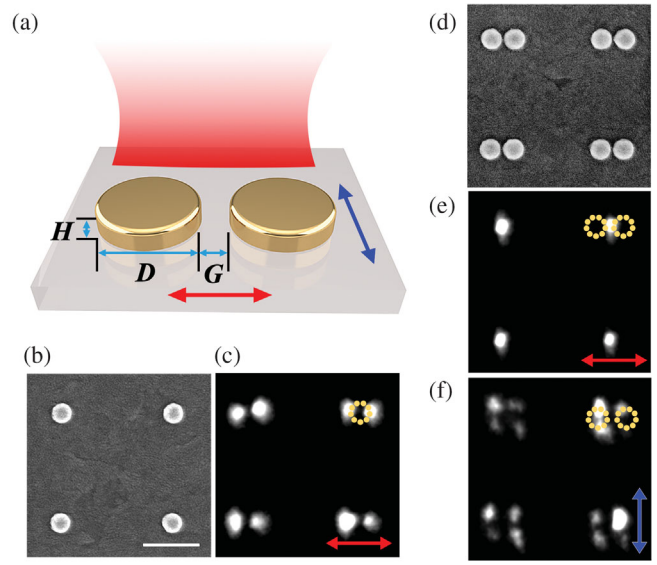

FIG. 1. Characterization of Au nanodisks and disk dimers. (a) Structure of Au disk dimer. D, H, and G are diameter, height, and gap size. The arrows indicate the polarization of the excitation light (longitudinal, red arrow; transverse, blue arrow). (b) SEM image of isolated disks, and (c) corresponding PEEM image at the dipole resonance wavelength of 760 nm. (d) SEM image of disk dimers with $G = 25$ nm, and corresponding PEEM images with (e) longitudinal and (f) transverse polarizations at respective resonance wavelengths of 850 and 750 nm. The positions of the disks are indicated by yellow circles. The scale bar indicates 500 nm.

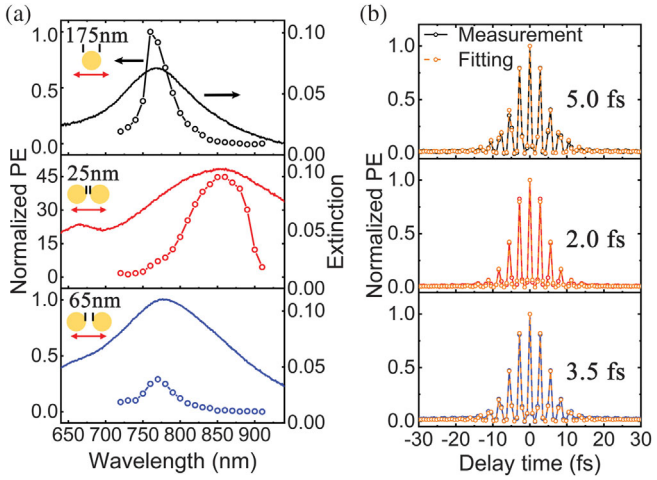

FIG. 2. Near-field and far-field properties and ultrafast dynamics from PEEM measurements with longitudinal polarization. (a) Near-field spectra (720–910 nm) normalized by the power and peak intensity of the isolated disks with corresponding far-field extinction spectra (640–940 nm). (b) Corresponding PE intensities as a function of delay time between pump and probe pulses with fitted dephasing times.

Au disk dimer is schematically shown in Fig. 1(a). Dimers are arranged in a two-dimensional square array over an area of 75×75 μm^2 with a pitch size of 1000 nm on an ITO coated glass substrate. Scanning electron microscopy (SEM) images of isolated disks and disk dimers with a gap size G of approximately 25 nm are shown in Figs. 1(b) and 1(d), respectively. PEEM measurements were employed to obtain near-field photoemission (PE) intensity distributions for the structures upon excitation by femtosecond laser pulses at the plasmon resonance wavelengths [20,21,25–27] (see Supplemental Material [33]). As shown later, the dipolar resonance of the Au disks peaked at 760 nm. The Au dimers exhibited two resonance modes, namely, longitudinal L and transverse T polarized modes corresponding to excitation light polarizations parallel and perpendicular to the dimer axis, respectively. For the Au dimers shown in Fig. 1(d), the peak wavelengths of the L and T modes are located at 850 and 750 nm, respectively. PEEM images of the isolated disks, for L-polarized excitation, and of the dimers, for both L- and T-polarized excitations, are shown in Figs. 1(c), 1(e), and 1(f), respectively. The PE intensity obtained by PEEM under laser excitation is directly correlated to the plasmonic near-field intensity in a nonlinear manner: PE $\propto I^N$, where I is the local electric field intensity and N is the nonlinear order of the PE. Therefore, the PEEM images can be regarded as displaying the near-field intensity distribution of the Au structures, and the PE intensity provides direct evidence of near-field enhancement [20,25,27]. Under L-polarized excitation, hot spots at both sides of the Au nanodisks, corresponding to the excitation of dipolar modes along the polarization direction, appear [Fig. 1(c)]. By contrast, because of the strong localized field enhancement in the gap upon excitation of L modes, for the dimers, only hot spots in the gap can be observed under these conditions [Fig. 1(e)]. When the polarization is changed to the transverse polarization, the hot spots in the gap disappear, to be replaced by hot spots at both sides of each disk [Fig. 1(f)] that are similar to the hot spots of the individual Au nanodisks, as a result of the excitation of T modes.

By recording the integrated PE intensity at different excitation wavelengths, wavelength-dependent PE intensity curves, referred to as near-field spectra, can be obtained [27,28,42], as indicated by lines and circular data points in Fig. 2(a). The averaged PE spectrum overlaps with that from individual disks, indicating the good homogeneity (see Supplemental Material [33]). The peaks of the near-field spectra are close to those of the far-field spectra [unbroken lines in Fig. 2(a)]. It should be noted that the PE intensity curves and the corresponding far-field spectra are not identical (see Supplemental Material [33]). The dipole resonance peaks for the longitudinal polarization occur at approximately 760 and 850 nm for the isolated disks and disk dimers with a gap size of approximately 25 nm, respectively, as shown in both the far-field and near-field spectra [upper and middle panels in Fig. 2(a)]. The large redshift of the peak wavelength of the disk dimers compared to that of the isolated disks is attributed to

strong dipole-dipole interactions between the two adjacent disks, and the less intense peak at the shorter wavelength of approximately 660 nm in the far-field spectrum [middle panel in Fig. 2(a)] corresponds to the quadrupole-quadrupole bonding mode, which has little contribution to our investigation. The near-field spectra were normalized by the excitation laser power and peak intensity of the isolated disks (see Supplemental Material [33]). The maximum integrated PE intensity over the entire PEEM image of disk dimers is a factor of ~45 times that of the isolated disks. The strong near-field enhancement for the disk dimers is ascribed to plasmon localization in the small gap region [43–46], as seen in the near-field mapping of the disk dimers [Fig. 1(e)]. We also noticed that the spectral linewidth for the disk dimers is much broader than that for the isolated disks, in both the far-field and near-field spectra, which implies that the disk dimers have shorter dephasing times even though the near-field enhancement is much stronger.

To compare the dephasing times of the isolated disks and disk dimers directly, in the time domain, the dynamic properties of the LSPRs were investigated by TR-PEEM and an interferometric pump-probe technique, using a laser source that delivers 7.0-fs laser pulses with a central wavelength of 840 nm and a wavelength range of 650–1050 nm (see Supplemental Material [33]). Pump and probe pulses with the same power were generated after passing through a Mach-Zehnder interferometer. Chirped mirrors and a wedge pair were used to compensate for dispersion to ensure that the pulse duration was approximately 7.0 fs. By sweeping the time delay with an interval of 0.7 fs (phase delay $\pi/2$ for 840 nm), a series of PE signals could be recorded. The nonlinear orders of the PE for the isolated disks and disk dimers are 3.5 and 3.9, respectively, as obtained from the ratio of PE intensities at the time delays of 0 and ∞ (where ∞ signifies a time delay sufficiently long for the pump and probe pulses to be well separated and for the plasmon field to decay to zero before the probe pulse arrives): $PE_0/PE_\infty = 2^{2N-1}$. These nonlinear orders are close to the values reported in the literature [20,27]. The larger nonlinear order for the disk dimers is probably owing to the much longer resonance wavelength and much stronger near-field enhancement of the dimers. The dephasing time was fitted by applying an analytical model to the experimental time-resolved PE signals (see Supplemental Material [33]). The fitted dephasing times of the isolated disks and disk dimers are 5.0 and 2.0 fs, respectively, as shown in the upper and middle panels of Fig. 2(b). These dephasing times from the TR-PEEM measurements are consistent with those calculated from the linewidths of the far-field spectra [33]. Combined with the near-field enhancement of the two structures, we find that the dephasing time for the disk dimer is much shorter than that for the isolated disk, despite its near-field enhancement being much stronger. Next, we consider dimers with a larger gap size, 65 nm; their near-field and far-field spectra are shown in the bottom panel of Fig. 2(a).

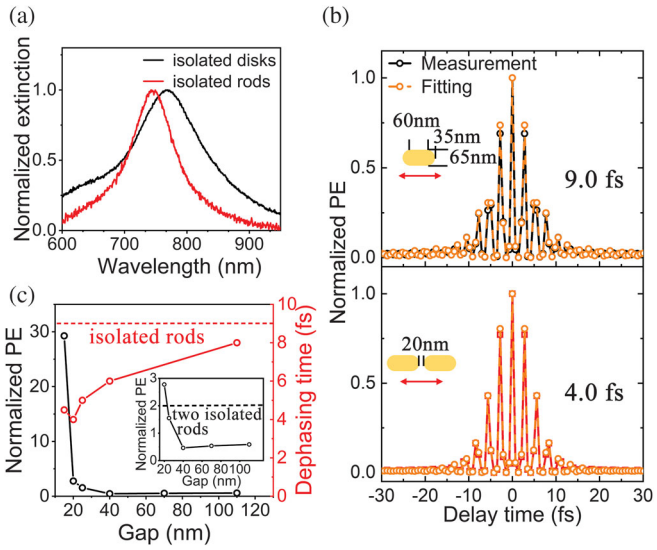

FIG. 3. Near-field properties and ultrafast dynamics of rod dimers from PEEM measurements with longitudinal polarization. (a) Comparison of normalized far-field extinction spectra for isolated disks and rods. (b) TR-PEEM measurements and fitting results for isolated rods and rod dimers with a gap size of 20 nm. (c) Gap-dependent PE intensities and dephasing times for rod dimers. The red dashed line denotes the dephasing time for the isolated rods. The inset in (c) shows an expanded view of the main plot, in which the PE intensity is normalized to that of the isolated rods.

It is extraordinary that the near-field enhancement for the dimers with $G = 65$ nm is even weaker than that of the isolated disks, while the dephasing time is shorter [lower panels, Figs. 2(a) and 2(b)]. The differences in the near-field enhancement and dephasing-time behaviors of dimers with gaps of 25 and 65 nm are related to the respective coupling between the two adjacent disks in each dimer and the plasmon localization in the gap region.

As plasmon coupling and plasmon localization are associated with gap size, gap-dependence measurements were performed. In order to verify whether the gap-size dependence of the near-field enhancement and dephasing time observed in the disk dimers is universal, measurements were performed on rod dimers. The isolated rods have a longer dephasing time than the disks, owing to their smaller volume with identical plasmon resonance wavelength [15]. The structures of the isolated rod and rod dimer are shown as insets in Fig. 3(b). For the longitudinal polarization [Fig. 3(a)], the isolated rods have narrower extinction-spectral linewidths than the isolated disks, and the dephasing time reaches 9.0 fs; while the dephasing time of the rod dimers with a 20-nm gap is much shorter, at only 4.0 fs [Fig. 3(b)]. The gap-dependence results are shown in Fig. 3(c). The PE intensity is normalized by the laser power and peak intensity of the isolated rods. Near-field enhancement decreases over the range of gap sizes from 110 to 40 nm, and then increases sharply for smaller gaps. The dephasing

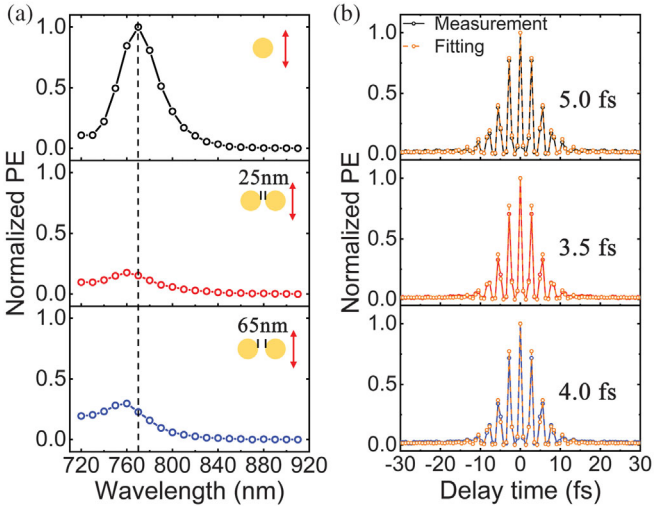

FIG. 4. Near-field properties (a) and ultrafast dynamics (b) of isolated disks and disk dimers from PEEM measurements with transverse polarization.

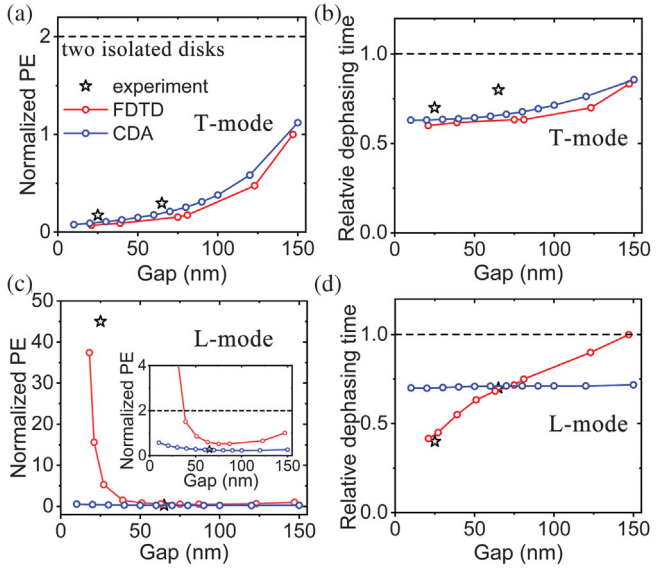

FIG. 5. Comparison of PE intensity and dephasing time for disk dimers from experiment, FDTD simulation, and CDA modeling. Normalized PE intensity and relative dephasing time as a function of gap size for disk dimers with transverse (a),(b), and longitudinal (c), (d) polarizations. The dashed lines denote the values for two isolated disks and the inset in (c) is an expanded view of the main plot.

time decreases from the value for the isolated rods (9.0 fs) to a limiting value at 4.0–4.5 fs for small gaps. The counterintuitive relationship between near-field enhancement and dephasing time is attributed to plasmon coupling and localization. We infer that at larger gap sizes, plasmon localization contributes little, and plasmon coupling dominates, inducing a faster radiative decay rate than that of the isolated particles owing to the coherent addition of their dipole moments, the so-called superradiance [47–49], leading to shorter dephasing times. However, under the same gap-size condition, near-field enhancement decreases owing to the loss of energy. When the gap is sufficiently small, the dominant cause of the near-field enhancement is plasmon localization in the gap region, which increases quickly as the gap size decreases. Importantly, the near-field enhancement induced by plasmon localization leads to further decreases in dephasing time, owing to enhanced radiative decay.

To distinguish between the individual effects of plasmon coupling and plasmon localization, we employed a simple method to separate their effects, using T-polarized laser excitation. For the T mode, there is no plasmon localization at the gap region, and only coupling exists. Continuing to use the disk dimer structures described above, for disk dimers with gap sizes of 25 and 65 nm, plasmon resonance peaks were obtained with small blueshifts from the peaks for the isolated disks, owing to the coupling between the two adjacent disks, as seen in the near-field spectra in Fig. 4(a). Interestingly, the near-field enhancement of the disk dimers is weaker than that of the isolated disks, and it decreases with gap size. Meanwhile, the dephasing times of the disk dimers with gap sizes of 25 and 65 nm are determined to be 3.5 and 4.0 fs, respectively, which are both shorter than that of the isolated disks, as shown in Fig. 4(b). In summary, in the absence of plasmon localization, near-field enhancement and dephasing times are affected only by coupling, which results in faster radiative decay rates, leading to shorter dephasing times and weaker near-field enhancement for the dimers with respect to the isolated disks, owing to the loss of energy. However, typically, for disk dimers with a designed gap size of 25 nm, the dephasing time for longitudinal polarization is significantly shorter than that of the transverse polarization, ranging from 3.5 to 2.0 fs. We attribute this difference to the effect of plasmon localization, because near-field enhancement induced by plasmon localization also promotes faster decay rates. In addition, the experimental results for both the longitudinal and transverse polarizations are well reproduced by finite-difference time-domain (FDTD) simulations (see Supplemental Material [33]). It is also observed, from the FDTD simulation results, that the plasmon damping of the dimer system is dominated by radiative decay because the scattering cross section is much larger than the absorption cross section.

To further demonstrate the effect of plasmon coupling on near-field enhancement and dephasing time, we adopted a coupled dipole approximation (CDA) model [50–53] (see Supplemental Material [33]). In the CDA model, each disk is approximated as a dipole. The near-field and far-field couplings are expressed as dipole radiation fields. The PE intensity and dephasing time are obtained as $|P|^8$ and the linewidth of $|P|^2$, respectively, where $|P|$ is the amplitude of the dipole moment. As each particle is simplified as a dipole, plasmon localization is not considered in this model. For the transverse polarization,

the plasmon localization effect is not significant because the excitation of the T mode in the dimer, and the CDA calculations are in good agreement with the results of the PEEM experiments and the FDTD simulations in the gap range up to 150 nm, as shown in Figs. 5(a) and 5(b). This implies that, for the T mode, the variation in near-field enhancement and dephasing time for the dimers is dominated by plasmon coupling between the two disks of each dimer. For the longitudinal polarization, the results obtained using the CDA model deviate significantly from the experimental and simulated results, as shown in Figs. 5(c) and 5(d), because the significant plasmon localization in the gap region is not considered in the CDA model. Although the CDA model is not a perfect model to calculate the near-field enhancement and the dephasing time in the present study, especially for the L modes, the model helps to discriminate the role of far-field and near-field plasmon coupling from the plasmon localization effect.

In conclusion, the correlation between near-field enhancement and dephasing time for dimer LSPRs in which plasmon damping is dominated by radiative decay has been investigated systematically. Employing TR-PEEM, we have studied the time-dependent and polarization-dependent properties of the dimer LSPRs, and these were well reproduced by FDTD simulations. We further distinguish the effect of near-field and far-field plasmon coupling from the plasmon localization effect by using a CDA model. In general, near-field and far-field coupling and plasmon localization together determine near-field enhancement and dephasing time. The strong near-field enhancement induced by plasmon localization enhances the decay rate, causing the dephasing time to decrease further from that induced by near-field and far-field coupling. Therefore, the effective dephasing time of dimers with strong near-field enhancement is much shorter than that of the corresponding isolated particles. In addition, the near-field enhancement of dimers may be weaker than that of isolated particles if the gap size is not sufficiently small, a factor which should be considered when designing such structures for SERS, optical trapping, and other related applications. This study should be further extended to an investigation of the correlation between near-field enhancement and dephasing time in other more complex plasmonic systems.

This work was supported by Japan Society for the Promotion of Science (JSPS) KAKENHI (Grants No. JP18H05205, No. JP17H01041, No. JP19H02737, and No. JP19H04667), the National Science Foundation of China (NSFC) (No. 11527901), and the National Key Research and Development Program of China (No. 2018YFA0704404). We acknowledge the support from the Nanotechnology Platform (Hokkaido University) and Dynamic Alliance for Open Innovation Bridging Human, Environment and Materials (Five-Star Alliance) of MEXT. This work was also supported by the Center for Emergent Functional Matter Science of National Chiao Tung University from the Featured Areas Research Center Program within the framework of the Higher Education Sprout Project by the Ministry of Education (MOE) in Taiwan.

[*]These authors contributed equally to this work.
[†]Corresponding author.
qhgong@pku.edu.cn
[‡]Corresponding author.
misawa@es.hokudai.ac.jp
[§]Present address: Department of Chemistry, Faculty of Science, Hokkaido University, Sapporo 060-0810, Japan.

[1] C. E. Talley, J. B. Jackson, C. Oubre, N. K. Grady, C. W. Hollars, S. M. Lane, T. R. Huser, P. Nordlander, and N. J. Halas, Nano Lett. **5**, 1569 (2005).
[2] Y. Zhang, Y. Zhen, O. Neumann, J. K. Day, P. Nordlander, and N. J. Halas, Nat. Commun. **5**, 4424 (2014).
[3] Y. Tanaka, S. Kaneda, and K. Sasaki, Nano Lett. **13**, 2146 (2013).
[4] M. L. Juan, M. Righini, and R. Quidant, Nat. Photonics **5**, 349 (2011).
[5] J. N. Anker, W. P. Hall, O. Lyandres, N. C. Shah, J. Zhao, and R. P. Van Duyne, Nat. Mater. **7**, 442 (2008).
[6] S. Lal, S. Link, and N. J. Halas, Nat. Photonics **1**, 641 (2007).
[7] Y. Nishijima, K. Ueno, Y. Yokota, K. Murakoshi, and H. Misawa, J. Phys. Chem. Lett. **1**, 2031 (2010).
[8] H. A. Atwater and A. Polman, Nat. Mater. **9**, 205 (2010).
[9] X. Shi, K. Ueno, T. Oshikiri, Q. Sun, K. Sasaki, and H. Misawa, Nat. Nanotechnol. **13**, 953 (2018).
[10] L. Zhou *et al.*, Science **362**, 69 (2018).
[11] K. L. Kelly, E. Coronado, L. L. Zhao, and G. C. Schatz, J. Phys. Chem. B **107**, 668 (2003).
[12] N. J. Halas, S. Lal, W. S. Chang, S. Link, and P. Nordlander, Chem. Rev. **111**, 3913 (2011).
[13] J. Ye, F. Wen, H. Sobhani, J. B. Lassiter, P. Van Dorpe, P. Nordlander, and N. J. Halas, Nano Lett. **12**, 1660 (2012).
[14] M. Hentschel, M. Saliba, R. Vogelgesang, H. Giessen, A. P. Alivisatos, and N. Liu, Nano Lett. **10**, 2721 (2010).
[15] C. Sönnichsen, T. Franzl, T. Wilk, G. von Plessen, J. Feldmann, O. Wilson, and P. Mulvaney, Phys. Rev. Lett. **88**, 077402 (2002).
[16] T. Klar, M. Perner, S. Grosse, G. von Plessen, W. Spirkl, and J. Feldmann, Phys. Rev. Lett. **80**, 4249 (1998).
[17] B. Foerster, V. A. Spata, E. A. Carter, C. Sönnichsen, and S. Link, Sci. Adv. **5**, eaav0704 (2019).
[18] S. Zhang, L. Chen, Y. Huang, and H. Xu, Nanoscale **5**, 6985 (2013).
[19] C. Y. Tsai, J. W. Lin, C. Y. Wu, P. T. Lin, T. W. Lu, and P. T. Lee, Nano Lett. **12**, 1648 (2012).
[20] Q. Sun, K. Ueno, H. Yu, A. Kubo, Y. Matsuo, and H. Misawa, Light Sci. Appl. **2**, e118 (2013).
[21] P. Melchior, D. Bayer, C. Schneider, A. Fischer, M. Rohmer, W. Pfeiffer, and M. Aeschlimann, Phys. Rev. B **83**, 235407 (2011).

[22] T. Hanke, G. Krauss, D. Träutlein, B. Wild, R. Bratschitsch, and A. Leitenstorfer, Phys. Rev. Lett. **103**, 257404 (2009).
[23] Y. Qin, B. Ji, X. Song, and J. Lin, Appl. Phys. B **125**, 3 (2019).
[24] E. Lorek *et al.*, Opt. Express **23**, 31460 (2015).
[25] H. Yu, Q. Sun, K. Ueno, T. Oshikiri, A. Kubo, Y. Matsuo, and H. Misawa, ACS Nano **10**, 10373 (2016).
[26] A. Kubo, K. Onda, H. Petek, Z. Sun, Y. S. Jung, and H. K. Kim, Nano Lett. **5**, 1123 (2005).
[27] Q. Sun, H. Yu, K. Ueno, A. Kubo, Y. Matsuo, and H. Misawa, ACS Nano **10**, 3835 (2016).
[28] F. Schertz, M. Schmelzeisen, R. Mohammadi, M. Kreiter, H. J. Elmers, and G. Schönhense, Nano Lett. **12**, 1885 (2012).
[29] E. Mårsell *et al.*, Nano Lett. **15**, 6601 (2015).
[30] M. Cinchetti, A. Gloskovskii, S. A. Nepjiko, G. Schönhense, H. Rochholz, and M. Kreiter, Phys. Rev. Lett. **95**, 047601 (2005).
[31] M. Aeschlimann, T. Brixner, A. Fischer, C. Kramer, P. Melchior, W. Pfeiffer, C. Schneider, C. Struber, P. Tuchscherer, and D. V. Voronine, Science **333**, 1723 (2011).
[32] B. Ji, X. Song, Y. Dou, H. Tao, X. Gao, Z. Hao, and J. Lin, New J. Phys. **20**, 073031 (2018).
[33] See Supplemental Material at http://link.aps.org/supplemental/10.1103/PhysRevLett.124.163901, in which we have given details on sample fabrication and characterization, PEEM measurement, near-field spectra normalization, dephasing time fitting, FDTD simulations, and CDA calculations. In the Supplemental Material, additional Refs. [34–41] are included.
[34] J. Zuloaga and P. Nordlander, Nano Lett. **11**, 1280 (2011).
[35] P. Alonso-González *et al.*, Phys. Rev. Lett. **110**, 203902 (2013).
[36] B. Lamprecht, J. R. Krenn, A. Leitner, and F. R. Aussenegg, Phys. Rev. Lett. **83**, 4421 (1999).
[37] P. B. Johnson and R. W. Christy, Phys. Rev. B **6**, 4370 (1972).
[38] J. D. Jackson, *Classical Electrodynamics* (John Wiley & Sons, New York, 1999).
[39] S. A. Maier, M. L. Brongersma, P. G. Kik, and H. A. Atwater, Phys. Rev. B **65**, 193408 (2002).
[40] H. Yu, Q. Sun, J. Yang, K. Ueno, T. Oshikiri, A. Kubo, Y. Matsuo, Q. Gong, and H. Misawa, Opt. Express **25**, 6883 (2017).
[41] I. Ragheb, M. Braik, A. Mezeghrane, L. Boubekeur-Lecaque, A. Belkhir, and N. Felidj, J. Opt. Soc. Am. B **36**, E36 (2019).
[42] L. Douillard, F. Charra, C. Fiorini, P. M. Adam, R. Bachelot, S. Kostcheev, G. Lerondel, M. L. de la Chapelle, and P. Royer, J. Appl. Phys. **101**, 083518 (2007).
[43] T. Atay, J. H. Song, and A. V. Nurmikko, Nano Lett. **4**, 1627 (2004).
[44] J. Zuloaga, E. Prodan, and P. Nordlander, Nano Lett. **9**, 887 (2009).
[45] H. Aouani, M. Rahmani, M. Navarro-Cía, and S. A. Maier, Nat. Nanotechnol. **9**, 290 (2014).
[46] A. E. Schlather, N. Large, A. S. Urban, P. Nordlander, and N. J. Halas, Nano Lett. **13**, 3281 (2013).
[47] R. H. Dicke, Phys. Rev. **93**, 99 (1954).
[48] C. Dahmen, B. Schmidt, and G. von Plessen, Nano Lett. **7**, 318 (2007).
[49] P. Olk, J. Renger, M. T. Wenzel, and L. M. Eng, Nano Lett. **8**, 1174 (2008).
[50] S. Zu, Y. Bao, and Z. Fang, Nanoscale **8**, 3900 (2016).
[51] Z. Fang, J. Cai, Z. Yan, P. Nordlander, N. J. Halas, and X. Zhu, Nano Lett. **11**, 4475 (2011).
[52] X. Lu, J. Wu, Q. Zhu, J. Zhao, Q. Wang, L. Zhan, and W. Ni, Nanoscale **6**, 14244 (2014).
[53] B. Auguié and W. L. Barnes, Phys. Rev. Lett. **101**, 143902 (2008).